Epidemic control in networks with cliques

L. D. Valdez,[1,*] L. Vassallo,[1] and L. A. Braunstein[1,2]
[1]*Instituto de Investigaciones Físicas de Mar del Plata (IFIMAR), Departamento de Física, FCEyN, Universidad Nacional de Mar del Plata–CONICET, Mar del Plata 7600, Argentina*
[2]*Physics Department, Boston University, Boston, Massachusetts 02215, USA*

(Received 26 December 2022; accepted 13 April 2023; published 22 May 2023)

Social units, such as households and schools, can play an important role in controlling epidemic outbreaks. In this work, we study an epidemic model with a prompt quarantine measure on networks with cliques (a *clique* is a fully connected subgraph representing a social unit). According to this strategy, newly infected individuals are detected and quarantined (along with their close contacts) with probability f. Numerical simulations reveal that epidemic outbreaks in networks with cliques are abruptly suppressed at a transition point f_c. However, small outbreaks show features of a second-order phase transition around f_c. Therefore, our model can exhibit properties of both discontinuous and continuous phase transitions. Next, we show analytically that the probability of small outbreaks goes continuously to 1 at f_c in the thermodynamic limit. Finally, we find that our model exhibits a backward bifurcation phenomenon.

DOI: 10.1103/PhysRevE.107.054304

I. INTRODUCTION

When a novel and dangerous disease unfolds, governments often implement a wide range of non-pharmaceutical interventions (NPIs) to decrease the burden on health care services [1–3]. These interventions include, for example, travel bans, quarantine measures, and school closures. Epidemiological studies have shown that the spread of contagious diseases depends on multiple factors, including the network of face-to-face contacts [4–6]. Therefore, studying the effect of different network structures on the spread of epidemics becomes essential to develop more effective interventions.

In the last few years, several mathematical models have been proposed to study NPIs in complex networks [7–10]. For example, St-Onge *et al.* [11,12] recently explored a susceptible-infected-susceptible (SIS) model on networks with cliques (defined as groups where all members are connected to each other) and proposed a mitigation strategy that consists of reducing the maximum clique size. They found that the total fraction of infected people decreases as the maximum clique size is reduced. Another NPI that has been extensively studied in the field of complex networks is the rewiring strategy, in which susceptible individuals protect themselves by breaking their links with infected contacts and creating new ones with noninfectious people [13]. Interestingly, recent work has shown that this strategy can lead to an explosive epidemic for a susceptible-infected-recovered (SIR) model [14,15].

Several works have also explored the effect of different quarantine strategies on the spread of epidemics [16–18]. For example, Hasegawa and Nemoto [18] investigated a susceptible-infected-recovered-quarantined (SIRQ) model with a "prompt quarantine strategy" that works as follows. At each time step, after individuals become infected, they are immediately detected with probability f, and then the detected ones and their contacts are placed under quarantine. In that work, they showed (for networks without cliques) that the probability of an epidemic and the proportion of recovered people undergo a continuous phase transition. On the other hand, very recently, Börner *et al.* [19] studied an SIRQ model with a quarantine strategy that becomes less effective over time. More specifically, they considered the case in which the rate at which individuals are quarantined decreases as the total number of infected people increases. For a mean-field model (corresponding to a homogeneously well-mixed population), they showed that the proportion of recovered people at the final stage could exhibit a discontinuous transition. However, they also observed that the probability of an epidemic vanishes continuously around this transition point, so their model exhibits features of both continuous and discontinuous phase transitions.

Following the line of research on nonpharmaceutical interventions, in this paper we investigate an SIRQ model with a prompt quarantine strategy on random networks with cliques. On the one hand, numerical simulations show that the probability of an epidemic (Π) vanishes continuously at a transition point $f = f_c$ (i.e., the probability of a small outbreak, $1 - \Pi$, goes to 1 at $f = f_c$). However, numerical simulations also reveal that the fraction of recovered people (R) is abruptly suppressed around $f = f_c$, so our model displays features of both continuous and discontinuous phase transitions as in [19]. Note that this result is markedly different from the case without cliques, where only a continuous phase transition was observed [18], as mentioned above. Finally, we find that our model exhibits the phenomenon of backward bifurcation. In order to elucidate the origin of these results, we explore the spread dynamics close to the transition point, and numerical

*ldvaldes@mdp.edu.ar

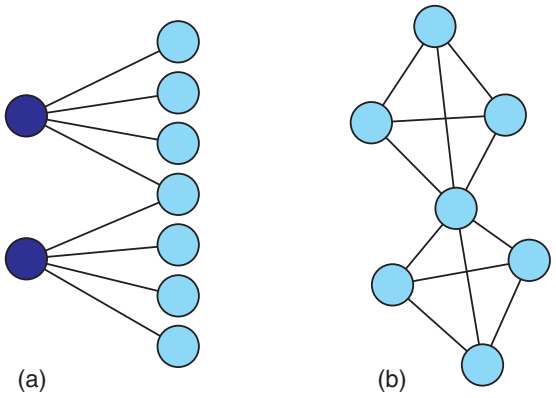

FIG. 1. Illustration of a bipartite network (a) and its projection (b). Each blue node represents a clique and each light blue node represents an individual.

simulations suggest that the quarantine strategy becomes less effective over time, which may explain why our model exhibits the same behavior as in [19].

This paper is organized as follows. In Sec. II, we describe the details of our model. In Secs. III A and III B, we investigate the final stage of an epidemic and the probability of small outbreaks ($1-\Pi$) when only one person is infected at the beginning of the outbreak. In the following section, we explore the final stage of an epidemic when a large proportion of the population is infected at the beginning of the spreading process. Finally, we present our conclusions.

II. MODEL DESCRIPTION

A. Network with cliques

Networks with cliques can be represented as bipartite networks (as illustrated in Fig. 1). In this work, we will focus on bipartite networks that are locally treelike because they have two main advantages. First, they can be easily generated by using a version of the configuration model [20,21], and, second, they simplify the analytical treatment, as explained in [22].

To generate these networks, we apply the following steps:

Step 1: We create two disjoint sets, denoted by I and C, where I corresponds to the set of individuals and C represents the set of cliques. The total numbers of individuals and cliques are denoted by N_I and N_C, respectively.

Step 2: We randomly assign a number k_I of cliques (or "stubs") to every person according to a probability distribution $P(k_I)$. Similarly, we assign a number k_C of individuals (or "stubs") to every clique according to a probability distribution $P(k_C)$. Initially, each stub is unmatched. We denote the total number of stubs in sets I and C, by $\mathcal{S}_I$ and $\mathcal{S}_C$, respectively. In the limit of large network sizes, the relation $\mathcal{S}_C = \mathcal{S}_I$ holds (as explained in [23]). Additionally, in this limit, we have that $\mathcal{S}_I = \langle k_I\rangle N_I$ and $\mathcal{S}_C = \langle k_C\rangle N_C$, where $\langle k_I\rangle = \sum_{k_I} k_I P(k_I)$ and $\langle k_C\rangle = \sum_{k_C} k_C P(k_C)$.

Step 3: In practice, for finite networks, if $|\mathcal{S}_C - \mathcal{S}_I| < 0.01\langle k_I\rangle N_I$ then we proceed as follows. We randomly choose one stub from each set and join them together to make a complete link (but avoiding multiple connections between individuals and cliques). This procedure is repeated until one of these sets is empty. On the other hand, if $|\mathcal{S}_C - \mathcal{S}_I| > 0.01\langle k_I\rangle N_I$, our algorithm returns to Step 1.

Step 4: Finally, we eliminate those stubs that remained unmatched from the previous step, and project the set of cliques onto the set of individuals, as illustrated in Fig. 1.

B. Susceptible-infected-recovered-quarantined model

Let us first introduce the susceptible-infected-recovered model (SIR), and some definitions.

The SIR model splits the population into three compartments called susceptible (S), infected (I), and recovered (R). Here, the symbols S, I, and R refer to both the state of an individual and the proportion of the population in each compartment, where $S + I + R = 1$. For a discrete-time SIR model, all individuals synchronously update their states according to the following rules. At each time step, $t \to t + 1$, every infected individual

(1) transmits the disease to each susceptible neighbor with probability β,

(2) recovers from the disease after being infected for t_r time steps (which is called the recovery time) and becomes permanently immune. In this paper, we will use $t_r = 1$.

Typically, the spreading process starts with a single infected individual, called the "index case," and the rest of the population is susceptible. The disease then spreads through the population until the system reaches a final stage with only susceptible and recovered individuals. If the disease dies out after a few time steps and only an insignificant fraction of the population has become infected, then such an event is defined as a small outbreak. Conversely, the outbreak turns into an epidemic if the fraction of recovered people is macroscopic at the final stage. In the last few years, several works have also studied the case in which a macroscopic fraction I_0 of the population is infected at the beginning of the spreading process [24–28]. This case is usually referred to as a nontrivial or large initial condition.

A widely used measure to predict whether a disease will develop into a small outbreak or an epidemic is the basic reproduction number R_0, defined as the average number of secondary cases infected by the index case [29]. For a value of R_0 less than 1, the probability of a disease becoming an epidemic is known to be zero ($\Pi = 0$), while, for R_0 greater than 1, this probability is positive ($\Pi > 0$). Finally, around $R_0 = 1$, there is a second-order phase transition where many quantities behave as power laws [30,31]. For example, at $R_0 = 1$ the probability distribution of the number of recovered individuals for small outbreaks, denoted by $P(s)$, decays algebraically as $P(s) \sim s^{-(\tau-1)}$, where τ is called the Fisher exponent [30].

As explained in the Introduction, an extension of the SIR model that was proposed in [18] introduces a Q compartment in order to study the effect of a prompt quarantine strategy on the epidemic spread. In this model, the states of the nodes were updated asynchronously. However, in our work, we will consider a synchronous version of that model in order to simplify the analytical study. More precisely, our model works as follows: at time t,

(1) All infected individuals are detected and isolated with probability f, i.e., they move to the Q compartment.

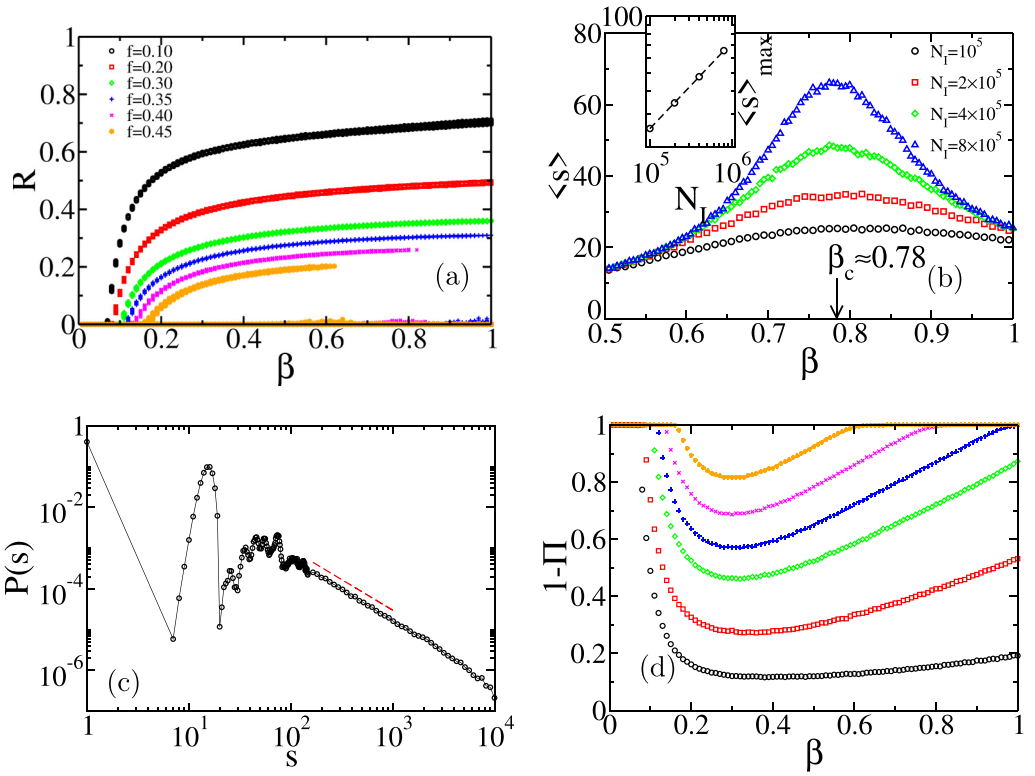

FIG. 2. (a) Scatter-plot of the fraction of recovered people at the final stage, R, as a function of β for a RR network with $k_C = 7$, $k_I = 3$, $N_I = 10^6$, and different values of the probability of detection f. Results were obtained from 10^3 stochastic realizations. (b) $\langle s \rangle$ against β for $f = 0.4$ and several values of N_I. Results were averaged over 10^5 realizations. The vertical arrow indicates the peak position β_c of $\langle s \rangle$ for $N_I = 8 \times 10^5$. In the inset, we show the height of the peak of $\langle s \rangle$, which we call $\langle s \rangle_{\max}$ (in log-log scale) for the same values of N_I as in the main plot. The dashed line corresponds to a power-law fit with an exponent of 0.46. (c) distribution $P(s)$ for $\beta = 0.78$, $f = 0.4$, and $N_I = 10^6$, obtained from 3×10^5 stochastic realizations (symbols). The solid black line is a guide to the eye, and the dashed red line is a power-law function with an exponent equal to $\tau - 1 = 1.5$. (d) Probability of a small outbreak, $1 - \Pi$, against β for the same parameter values as in panel (a). Results were averaged over 10^5 stochastic realizations.

(2) Next, all the neighbors of the individuals who were isolated in the previous step, also move to the Q compartment.

(3) After that, those infected individuals who have not been isolated, will transmit the disease to each susceptible neighbor with probability β.

(4) Finally, individuals who are still in the I compartment and have been infected for t_r time steps, will recover [32]. Likewise, people who have been infected and then quarantined will move to the R compartment after t_r time steps, so R represents the proportion of the population ever infected. In this paper, we present results only for $t_r = 1$; however, we have verified that our findings remain qualitatively unchanged for $t_r > 1$ (not shown here).

Similarly to the standard SIR model, at the final stage of the SIRQ model the population consists solely of susceptible, recovered, and quarantined individuals.

Note that, according to the rules of our model, it is sufficient to detect a single infected person in a clique to quarantine the entire clique. Therefore, larger (smaller) cliques have a higher (lower) probability of being quarantined. On the other hand, from one perspective, our model could be seen as a spreading process in higher-order networks [33,34] because the transition from a susceptible to a quarantined state is not caused by pairwise interactions but rather by group interactions. Typically, in models with higher-order structures, nodes become "infected" through group interactions, and after that, they transmit the "infection" to other nodes. However, it should be noted that in our model quarantined individuals are removed from the system, so they cannot transmit their state to the rest of the population, unlike other contagion models with higher-order structures.

In the following sections, we will study our SIRQ model on networks with cliques.

III. RESULTS

A. Final stage

In this section, we investigate the final stage of the SIRQ model for random regular (RR) networks with cliques, defined as networks in which every clique has k_C members and every individual belongs to k_I cliques. We will show numerical results for RR with $k_I = 3$, and $k_C = 7$ and focus only on the case where a single individual is infected at the beginning of the dynamic process. In Appendix B, we present additional results for networks in which k_C and k_I follow other probability distributions.

In Fig. 2(a), we show a scatter plot of R vs β for several values of the probability of detection f. For low values of f, we observe that the transition from an epidemic-free phase to an epidemic phase is continuous. However, for $f \gtrsim 0.35$

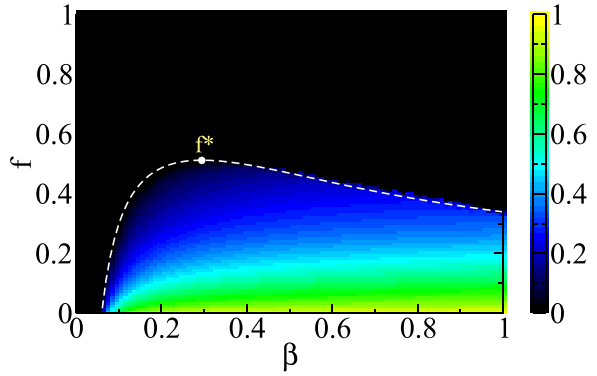

FIG. 3. Heat-map of R in the plane β-f for RR networks with cliques (with $k_C = 7$ and $k_I = 3$), obtained from numerical simulations. To compute R, we took into account only those realizations in which an epidemic occurs ($R > 1\%$). Darker colors represent a low value of R (black corresponds to $R = 0$) and brighter colors a higher value of R (yellow corresponds to $R = 1$). Simulation results were averaged over 10^3 stochastic realizations with $N_I = 10^5$. The dashed white line was obtained from Eq. (1) for $R_0 = 1$, and the point $f^* = 0.51$ corresponds to the value of f above which the system is in an epidemic-free phase for any value of β.

we see that, as β increases, another phase transition exists above which the fraction of recovered individuals is abruptly suppressed. This transition is also observed in other network topologies (see Appendix B), especially in networks containing larger cliques. In Sec. III C, we will show that around this transition point, a backward bifurcation occurs.

To delve deeper into the nature of the transition point at which R is abruptly suppressed, we will study how small outbreaks behave around this point. Here, we consider that a small outbreak occurs when the fraction of the recovered people is below 1% at the final stage. Figure 2(b) shows the average number of recovered individuals for small outbreaks $\langle s \rangle$ vs β for $f = 0.4$. Interestingly, we note that $\langle s \rangle$ exhibits a peak around a value of β that we call β_c, which roughly corresponds to the point at which R is abruptly suppressed [see Fig. 2(a)]. Furthermore, the height of this peak increases with N_I as a power law [see the inset of Fig. 2(b)], which is a typical finite-size effect of a second-order phase transition [30]. On the other hand, Fig. 2(c) shows the probability distribution of the number of recovered individuals for outbreaks at $\beta = \beta_c$. It can be seen that $P(s)$ decays as a power law. Finally, in Fig. 2(d), we display the probability of a small outbreak, $1 - \Pi$, as a function of β (note that Π is the probability that an epidemic occurs), and we get that $1 - \Pi$ goes continuously to 1 around $\beta = \beta_c$, which again is a feature of other epidemic and percolation models in random networks with a continuous phase transition [35,36]. Therefore, if we take together the results of Figs. 2(b)–2(d), they all suggest that quantities associated with small outbreaks will exhibit properties of a continuous phase transition.

To provide a broader picture of the effect of our strategy on networks with cliques, in Fig. 3 we show the heat map of R when an epidemic occurs in the plane β-f. From this figure, we observe that there is a minimum detection probability f^*, above which the system is always in an epidemic-free phase. On the other hand, we also find that in the region $\beta \lesssim 1$ an abrupt color change occurs around $f \approx 0.4$, which indicates that the system undergoes a discontinuous transition in that region of the parameter space.

Next, we will compute the basic reproduction number, R_0. As mentioned in Sec. II B, R_0 is a widely used quantity to predict whether a disease outbreak will become an epidemic or die out quickly, and typically, around $R_0 = 1$, a second-order phase transition occurs. In order to estimate R_0, we adapt the approach proposed in [37], leading us to the following expression for RR networks with cliques:

$$R_0 = \frac{\epsilon_1 + \epsilon_2}{\beta(k_C - 1)}, \tag{1}$$

with

$$\epsilon_1 = (k_C - 1)(1 - \beta)[(\beta(1 - f) + (1 - \beta))^{k_C - 2} - (\beta(1 - \beta)(1 - f) + (1 - \beta))^{k_C - 2}], \tag{2}$$

$$\epsilon_2 = (1 - f)(1 - \beta f)^{k_C - 2}(k_I - 1)(k_C - 1)^2\beta^2. \tag{3}$$

In Eq. (1),

(1) The denominator is the average number of individuals (within a clique) who are infected by the index case. We refer to these individuals as the "first generation."

(2) The numerator corresponds to the average number of people who are infected by the first generation. In Appendix A, we explain how to derive the expressions of ϵ_1 and ϵ_2.

In Fig. 3, we plot the set of points (β_c, f_c) that satisfy the constraint $R_0 = 1$. In particular, for $\beta_c = 1$, it can be easily obtained from Eq. (1) that f_c is given by

$$f_c = 1 - \left(\frac{1}{(k_I - 1)(k_C - 1)}\right)^{\frac{1}{k_C - 1}}. \tag{4}$$

Remarkably, from Fig. 3, we can see that the predicted curve agrees well with the entire boundary between the epidemic and epidemic-free phases, including in the region where a discontinuous transition occurs. In Sec. III C, we will see that this result is consistent with a backward bifurcation phenomenon around $R_0 = 1$.

In summary, in this section we found that the SIRQ model on networks with cliques has a discontinuous phase transition, but at the same time several quantities [specifically, $\langle s \rangle$, $1 - \Pi$, and $P(s)$] display the same features of a continuous phase transition. We note, however, that the results shown in this section were obtained from simulations in finite networks and from approximate formulas. In the following section, we will demonstrate that in the thermodynamic limit ($N_I \to \infty$) the probability of a small outbreak ($1 - \Pi$) goes continuously to 1 at the transition point for $\beta = 1$.

B. Probability of a small outbreak

In this section, we will describe the SIRQ model as a forward branching process [35,38] to calculate the probability of a small outbreak, $1 - \Pi$, and the transition point $f = f_c$ for $\beta = 1$. Here, we focus only on RR networks with cliques, but in Appendix C we compute these quantities for other network structures.

Branching theory has been extensively applied to the study of many processes on random networks, including cascading failures [39,40], disease transmission [23,41,42], random percolation [43,44], k-core percolation [45,46], and fractional percolation [47,48]. For an SIR model, this theory was first applied to networks without cliques to calculate the behavior of various quantities as a function of β [23,41]. Later on, multiple works used branching theory to study the SIR model on networks with cliques [49–52]. However, their calculations were usually more complex because they required an exhaustive enumeration of transmission events occurring within a clique with at least one infected person. But, for $\beta = 1$, these calculations can be substantially simplified. This is because, when individuals become infected (in a clique composed of susceptible members), at the next time step they will transmit the disease to the rest of the clique members with probability 1, unless an intervention strategy is applied. Therefore, in what follows, we will focus only on the case $\beta = 1$.

To compute the probability of a small outbreak, $1 - \Pi$, we first need to calculate the probability ϕ that an infected individual (reached through a link) will not generate an epidemic [35,36]. By using the branching process approach, it can be found that ϕ is the solution of the following self-consistent equation:

$$\phi = [((1-f)\phi)^{k_C-1} + 1 - (1-f)^{k_C-1}]^{k_I-1}. \tag{5}$$

The left-hand side (l.h.s.) of this equation is the probability that an infected individual "j" reached through a link does not cause an epidemic. On the other hand, the right-hand side (r.h.s.) is the probability that an infected individual "j" transmits the disease, but none of the $k_I - 1$ outgoing cliques will be able to cause an epidemic. This is because one of the following two events happens to every clique:

(1) with probability $1 - (1-f)^{k_C-1}$, at least one member (other than "j") is detected, so the whole clique is placed under quarantine,

(2) with probability $[(1-f)\phi]^{k_C-1}$, none of its members are detected but also they will not be able to generate epidemics.

After solving Eq. (5), the probability $1 - \Pi$ that an index case does not cause an epidemic can be obtained from the equation

$$1 - \Pi = f + (1-f)[((1-f)\phi)^{k_C-1} + 1 - (1-f)^{k_C-1}]^{k_I}, \tag{6}$$

where, in the r.h.s.,

(1) the first term corresponds to the probability that the index case is detected,

(2) the second term corresponds to the scenario where the index case is not detected and transmits the disease, but none of the k_I outgoing cliques will be able to generate an epidemic, similarly to Eq. (5).

It is worth noting that Eqs. (5) and (6) are valid only if the initial fraction of index cases is infinitesimal.

Another quantity of interest that can be calculated in the limit of large network sizes is the critical threshold f_c at which a phase transition occurs. To derive f_c, we take derivatives of both sides of Eq. (5) at $\phi = 1$ and obtain

$$f_c = 1 - \left(\frac{1}{(k_I - 1)(k_C - 1)}\right)^{\frac{1}{k_C-1}}, \tag{7}$$

which has the same expression as in Eq. (4).

To verify the validity of our theoretical analysis, we performed numerical simulations of the SIRQ model on RR networks with cliques. In Fig. 4(a), we show the mean size of small outbreaks $\langle s \rangle$ vs f for different network sizes (N_I). It can be seen that, as N_I increases, the peak position of $\langle s \rangle$ [that we call $f_c(N_I)$] converges to the critical threshold f_c predicted by Eq. (7). On the other hand, in Fig. 4(b), we display the probability of a small outbreak, $1 - \Pi$, obtained from our simulations and theoretical predictions [see Eqs. (5) and (6)]. As seen in this figure, the agreement between theory and simulation is excellent. In addition, we observe that $1 - \Pi$ goes continuously to 1 (i.e., $\Pi \to 0$) at the critical threshold $f = f_c$ predicted by Eq. (7). Thus, our findings in this section provide further evidence that small outbreaks display features of a continuous phase transition around $f = f_c$, as noted in the previous section.

In the next section, we will investigate the effect of nontrivial initial conditions on the final stage of the propagation process and discuss the mechanism leading to the discontinuous transition observed in Sec. III A.

C. Backward bifurcation

In previous sections, we focused our attention only on the case where a single index case was infected at the beginning of the outbreak. Here, we will study the effect of a nontrivial initial condition on the final stage of the propagation process. To this end, we conduct numerical simulations in which the fraction of infected individuals at $t = 0$ (denoted by I_0) is macroscopic. In particular, we are interested only in the case where $f > f_c$ (i.e., $R_0 < 1$) because for $f < f_c$ (i.e., $R_0 > 1$) we have already found that an epidemic can take off even from a single index case (see Sec. III B).

Figure 5 shows a scatter-plot of the proportion of recovered people R at the final stage as a function of I_0 for $\beta = 1$ and $f = 0.40$ (which is greater than $f_c = 0.3391$; see Sec. III B), and for several network sizes N_I. Additionally, in the inset, we plot the average value of R vs f for the same parameter values used in the main plot. Interestingly, we obtain that R has an abrupt jump around $I_0 \approx 2.5 \times 10^{-3} \equiv I_0^*$. Therefore, our numerical simulations reveal that the final fraction of recovered people strongly depends on the initial fraction of infected individuals for $R_0 < 1$. In the language of bifurcation theory, these findings imply that our model undergoes a backward bifurcation [53], i.e., the final fraction of recovered people is bistable for $R_0 < 1$ ($f > f_c$). In Appendix D, we present additional results showing that the system is also bistable for other values of f and network topologies.

Previous studies have shown that this type of bifurcation can be caused by multiple mechanisms, such as exogenous reinfection and the use of an imperfect vaccine against infection [53]. On the other hand, very recently, Börner *et al.* [19] proposed a mean-field SIRQ model to explore different quarantine measures whose effectiveness decreases over time. Although not explicitly mentioned in that work, it can be seen

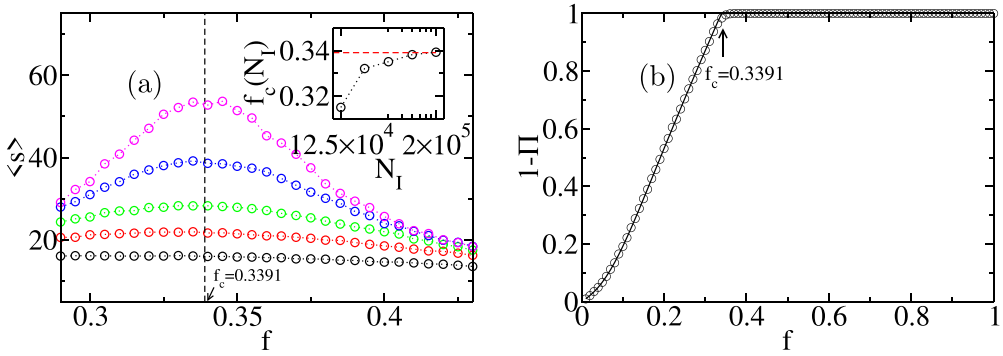

FIG. 4. (a) $\langle s \rangle$ vs f for $\beta = 1$ and RR networks with cliques ($k_C = 7$ and $k_I = 3$) for different network sizes (from bottom to top: $N_I = 1.25 \times 10^4$, 2.5×10^4, 5×10^4, 10^5, and 2×10^5). Symbols correspond to simulation results averaged over 10^5 stochastic realizations. The vertical dashed line indicates the predicted value of f_c obtained from Eq. (7). In the inset, we show the peak position of $\langle s \rangle$ (estimated from the main plot), called $f(N_I)$, as a function of N_I in a linear-log scale. The dashed line corresponds to our theoretical prediction of f_c. Dotted lines are a guide to the eye. (b) Probability of a small outbreak $(1 - \Pi)$ vs f for $\beta = 1$ and RR networks with cliques ($k_C = 7$ and $k_I = 3$). The line corresponds to the theory given by Eqs. (5) and (6), and symbols are simulation results averaged over 10^5 realizations with $N_I = 10^6$.

that their model is sensitive to initial conditions for $R_0 < 1$. Thus, a backward bifurcation phenomenon can also be caused by a quarantine measure that becomes less effective over time. Additionally, in [19], it was shown that a discontinuous epidemic phase transition occurs, and the probability of an epidemic vanishes around the transition point.

To explain why our model is sensitive to initial conditions for $R_0 < 1$, we will next measure the time evolution of $\langle n \rangle$ for several values of I_0, where $\langle n \rangle$ is defined as the average number of members (either in a susceptible or infected state) in a clique. In particular, for RR networks with cliques, the inequality $\langle n \rangle \leqslant k_C$ holds. From Fig. 6, we can clearly see that $\langle n \rangle$ is a decreasing function with time, or in other words, cliques become smaller as the population moves into the Q and R compartments. This leads us to the conclusion that the effectiveness of our strategy diminishes over time (as in [19]) because, as indicated in Sec. II B, smaller cliques are less likely to be placed under quarantine. Therefore, based on what was observed in [19], we conjecture that a decrease in $\langle n \rangle$ over time could explain why our model displays an abrupt transition and a backward bifurcation diagram, as seen in Secs. III A and III C, respectively.

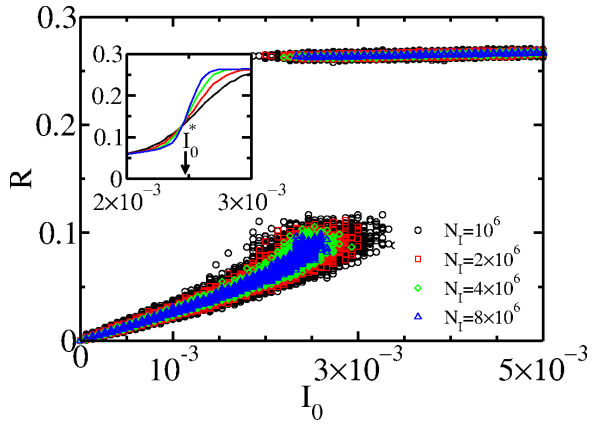

FIG. 5. Scatter plot of R vs I_0 obtained from numerical simulations for $\beta = 1$ and $f = 0.40$ in a RR network with $k_C = 7$, $k_I = 3$, and different network sizes N_I. Inset: Average value of R as a function of I_0 for the same parameter values used in the main plot. Numerical results were averaged over 10^4 stochastic realizations. The vertical arrow indicates the value of I_0^* around which R undergoes a phase transition.

IV. CONCLUSIONS

In summary, in this paper, we have investigated an SIRQ model with a prompt quarantine measure on networks with cliques. Numerical simulations revealed that epidemics could be abruptly suppressed at a critical threshold f_c, especially on networks with larger cliques (as shown in Appendix B). In contrast, we observed that small outbreaks exhibit properties of a continuous phase transition around f_c. Furthermore, using branching theory, we demonstrated that the probability of a small outbreak goes continuously to 1 at $f = f_c$ for $\beta = 1$. Therefore, these results indicate that our model can exhibit features of both continuous and discontinuous transitions. Next, we explored the impact of a macroscopic fraction of infected population at the beginning of the epidemic outbreak, and found that for $R_0 < 1$ a backward bifurcation phenomenon emerges. Finally, numerical simulations showed that the quarantine measure becomes less effective over time, which could explain why our model exhibits an abrupt transition and a backward bifurcation phenomenon.

Several lines of research can be derived from this work. For example, one question that remains open is whether the fraction of recovered people (in the event of an epidemic) can be predicted by branching theory since in this paper we have only used this theory to study small outbreaks. On the other hand, our model could be extended to include a time lag between infection and detection. Another relevant modification would be to allow quarantined individuals to return to the network after a certain period of time (especially those who were susceptible) because it is unrealistic to assume that they will remain isolated until the end of an epidemic outbreak. Additionally, a natural extension of our work would be to study the phenomenon of mesoscopic localization [11,12]. Lastly, our model could be studied in higher-order networks with simplicial complexes. It is known that simplicial contagion models can lead to explosive epidemic transitions [33,34], so

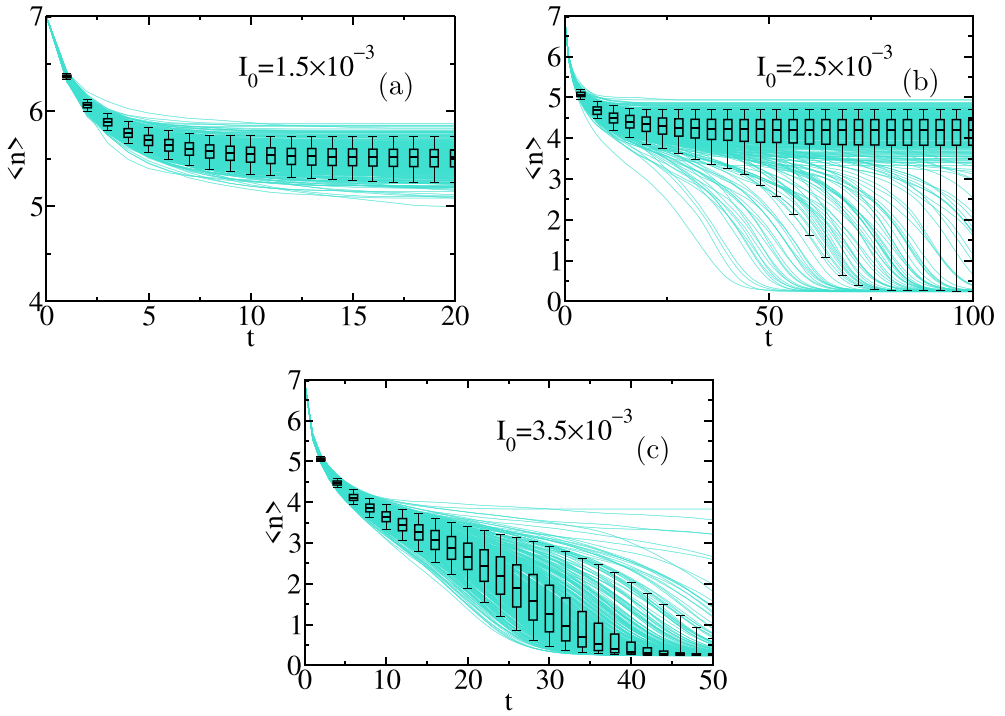

FIG. 6. Time evolution of the average number of individuals (either in a susceptible or infected state) in a clique, denoted by $\langle n \rangle$, for $f = 0.40$, $\beta = 1$, and several initial conditions: $I_0 = 1.5 \times 10^{-3}$ (a), $I_0 = 2.5 \times 10^{-3}$ (b), and $I_0 = 3.5 \times 10^{-3}$ (c). We generated 500 simulation trajectories (light blue lines) on RR networks with $k_C = 7$, $k_I = 3$, and $N_I = 10^6$. Box plots show the 5th, 25th, 50th, 75th and 95th percentile values of $\langle n \rangle$.

it would be interesting to investigate how they compete with a prompt quarantine measure. We will explore some of these extensions in a forthcoming work.

ACKNOWLEDGMENTS

We thank UNMdP (EXA 956/20), FONCyT (PICT 1422/2019) and CONICET, Argentina, for financial support. We also thank Dr. C. E. La Rocca and Lic. I. A. Perez for valuable discussions.

APPENDIX A: BASIC REPRODUCTION NUMBER FOR RR NETWORKS WITH CLIQUES

In [37], Miller estimated the basic reproduction number R_0 for random networks with cliques using the concept of rank proposed by Ludwing [54]. He found that R_0 can be well estimated by the following expression:

$$R_0 = \frac{\langle N_2 \rangle}{\langle N_1 \rangle}, \tag{A1}$$

where $\langle N_1 \rangle$ and $\langle N_2 \rangle$ are the average numbers of infected people of rank 1 and 2, respectively.

In our work, we use a similar approach to the one proposed in [37], but estimate R_0 as the following ratio:

$$R_0 = \frac{\langle \mathcal{N}_2 \rangle}{\langle \mathcal{N}_1 \rangle}, \tag{A2}$$

where

(1) $\langle \mathcal{N}_1 \rangle$ is the average number of people (within a clique) infected by the index case, that we call the "first generation,"

(2) $\langle \mathcal{N}_2 \rangle$ is the average total number of individuals infected by the people from the first generation.

In what follows, we derive the expressions of $\langle \mathcal{N}_1 \rangle$ and $\langle \mathcal{N}_2 \rangle$ for the case of random RR networks in which every clique has k_C members, and each person belongs to k_I cliques.

1. Derivation of $\langle \mathcal{N}_1 \rangle$

Let us consider that, at time $t = 0$, there is a single index case and the rest of the population is susceptible. If we assume that the index case is not detected, it follows that the probability that the index case will transmit the disease to $\mathcal{N}_1$ individuals (in a clique with k_C members) is given by

$$P(\mathcal{N}_1) = \binom{k_C - 1}{\mathcal{N}_1} \beta^{\mathcal{N}_1} (1-\beta)^{k_C - 1 - \mathcal{N}_1}. \tag{A3}$$

Then, the average number of people infected by the index case at $t = 1$ is

$$\begin{aligned} \langle \mathcal{N}_1 \rangle &= \sum_{\mathcal{N}_1 = 0}^{k_C - 1} \mathcal{N}_1 P(\mathcal{N}_1), \\ &= (k_C - 1)\beta. \end{aligned} \tag{A4}$$

Note that the people who get infected at this time step are at a chemical distance of $\ell = 1$ from the index case.

2. Derivation of $\langle \mathcal{N}_2 \rangle$

After the index case has infected $\mathcal{N}_1$ people, one of the following two events can occur:

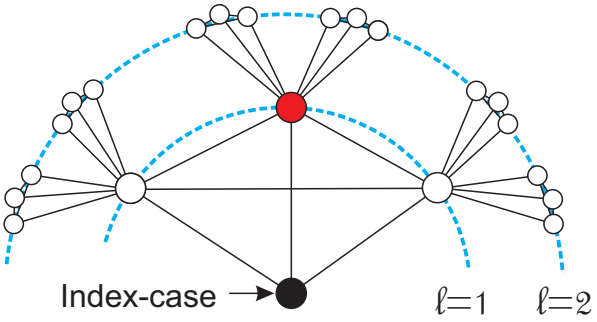

FIG. 7. Illustration of an index case (black node) who has infected one neighbor (red node) in a given clique at $t = 1$. In this example (i) the index case is already in a recovered state, (ii) cliques have $k_C = 4$ members, and (iii) each member belongs to $k_I = 3$ cliques. Blue dashed lines indicate the chemical distance from each node to the index case. Note that there are still $k_C - 1 - 1 = 2$ susceptible members (white nodes) at a chemical distance of $\ell = 1$ from the index case.

(1) At least one of these $\mathcal{N}_1$ individuals is detected, so the entire clique is isolated. The probability of this event is $P(D|\mathcal{N}_1) \equiv 1 - (1 - f)^{\mathcal{N}_1}$.

(2) No individual is detected, which occurs with probability

$$P(\neg D|\mathcal{N}_1) = 1 - P(D|\mathcal{N}_1) = (1 - f)^{\mathcal{N}_1}. \tag{A5}$$

If the second event occurs, people from the first generation will transmit the disease to every susceptible neighbor with probability β. As shown in the schematic illustration (see Fig. 7), these neighbors can be at a chemical distance of either $\ell = 1$ or $\ell = 2$ from the index case. Therefore, we split the average number of infected individuals at time $t = 2$, denoted by $\langle \mathcal{N}_2 \rangle$, as

$$\langle \mathcal{N}_2 \rangle = \epsilon_1 + \epsilon_2, \tag{A6}$$

where ϵ_1 (ϵ_2) corresponds to the number of new infected people at a chemical distance of $\ell = 1$ ($\ell = 2$) from the index case at time $t = 2$. In what follows, we will deduce the expressions of ϵ_1 and ϵ_2.

a. Deduction of ϵ_2

Let us assume that there are $\mathcal{N}_1$ infected people in the first generation, and none of them have been detected. This event occurs with probability $P(\mathcal{N}_1)P(\neg D|\mathcal{N}_1)$ [see Eqs. (A3) and (A5)]. As illustrated in Fig. 7, every infected person of the first generation has $k_I - 1$ outgoing cliques, each containing $k_C - 1$ susceptible individuals. Therefore, following similar arguments leading up to Eq. (A4), we obtain that every infected person of the first generation will transmit the disease (on average) to $(k_I - 1)(k_C - 1)\beta$ people at a distance of $\ell = 2$ from the index case.

Then, it follows that the average total number of infected individuals at a distance of $\ell = 2$ is given by

$$\begin{aligned}\epsilon_2 &= \sum_{\mathcal{N}_1=0}^{k_C-1} (k_I - 1)(k_C - 1)\beta \mathcal{N}_1 P(\mathcal{N}_1) P(\neg D|\mathcal{N}_1), \\ &= (1 - f)(1 - \beta f)^{k_C-2}(k_I - 1)(k_C - 1)^2\beta^2. \end{aligned} \tag{A7}$$

TABLE I. Cases considered in Figs. 11(a) and 11(b).

Case	$P(k_C)$	$P(k_I)$	$\langle k_C \rangle$	VAR(k_C)
I	Pois(3, 0, 20)	Pois(3, 0, 20)	3	3
II	Pois(7, 0, 20)	Pois(3, 0, 20)	7	7
III	Pois(7, 0, 20)	Pois(7, 0, 20)	7	7
IV	PL(2.0, 2, 100)	Pois(3, 0, 20)	6.4	112.4
V	PL(1.5, 2, 100)	Pois(3, 0, 20)	12.4	319.5

b. Deduction of ϵ_1

As illustrated in Fig. 7, there are $k_C - 1 - \mathcal{N}_1$ susceptible members at a chemical distance of $\ell = 1$ from the index case at $t = 1$. It is easy to see that, at the following time step, the effective probability of infection for any of these members is

$$p \equiv 1 - (1 - \beta)^{\mathcal{N}_1}. \tag{A8}$$

Then, if we denote by $\mathcal{N}_2$ the number of these members who get infected at $t = 2$, we have that the probability $P(\mathcal{N}_2|\mathcal{N}_1)$ can be written as

$$P(\mathcal{N}_2|\mathcal{N}_1) = \binom{k_C - 1 - \mathcal{N}_1}{\mathcal{N}_2} p^{\mathcal{N}_2}(1 - p)^{k_C - 1 - \mathcal{N}_1 - \mathcal{N}_2}. \tag{A9}$$

Finally, using Eqs. (A8) and (A9), we can estimate the average number of people becoming infected at time $t = 2$ as

$$\epsilon_1 = \sum_{\mathcal{N}_1=0}^{k_C-1} \sum_{\mathcal{N}_2=0}^{k_C-1-\mathcal{N}_1} \mathcal{N}_2 P(\mathcal{N}_2|\mathcal{N}_1)(1 - f)^{\mathcal{N}_1} P(\mathcal{N}_1), \tag{A10}$$

where the factor $(1 - f)^{\mathcal{N}_1} P(\mathcal{N}_1)$ is the probability that the first generation is composed of $\mathcal{N}_1$ infected individuals and none of them have been detected. Replacing Eqs. (A3) and (A9) in the last expression, and after algebraic manipulation, we obtain

$$\begin{aligned}\epsilon_1 = (k_C - 1)(1 - \beta)[&[\beta(1 - f) + (1 - \beta)]^{k_C-2} \\ &- [\beta(1 - \beta)(1 - f) + (1 - \beta)]^{k_C-2}]. \end{aligned} \tag{A11}$$

APPENDIX B: ADDITIONAL RESULTS

In Sec. III A, we investigated an SIRQ model on random networks with cliques and showed results for $P(k_C) = \delta_{k_C,7}$ and $P(k_I) = \delta_{k_I,3}$, where δ is the Kronecker delta. In what follows, we will study this SIRQ model for other $P(k_C)$ and $P(k_I)$ distributions.

1. RR networks with cliques

Here we will present our results for RR networks with
case I: $P(k_C) = \delta_{k_C,3}$ and $P(k_I) = \delta_{k_I,7}$,
case II: $P(k_C) = \delta_{k_C,5}$ and $P(k_I) = \delta_{k_I,2}$,
case III: $P(k_C) = \delta_{k_C,2}$ and $P(k_I) = \delta_{k_I,5}$.
For the simulations, only one person is infected at the beginning of the dynamic process.

In Figs. 8(a), 8(c), and 8(e), we show a scatter plot of the fraction of recovered people R at the final stage as a function of β for several values of f. Similarly, in Figs. 8(b), 8(d), and 8(f), we show R at the final stage as a function of f for different values of β.

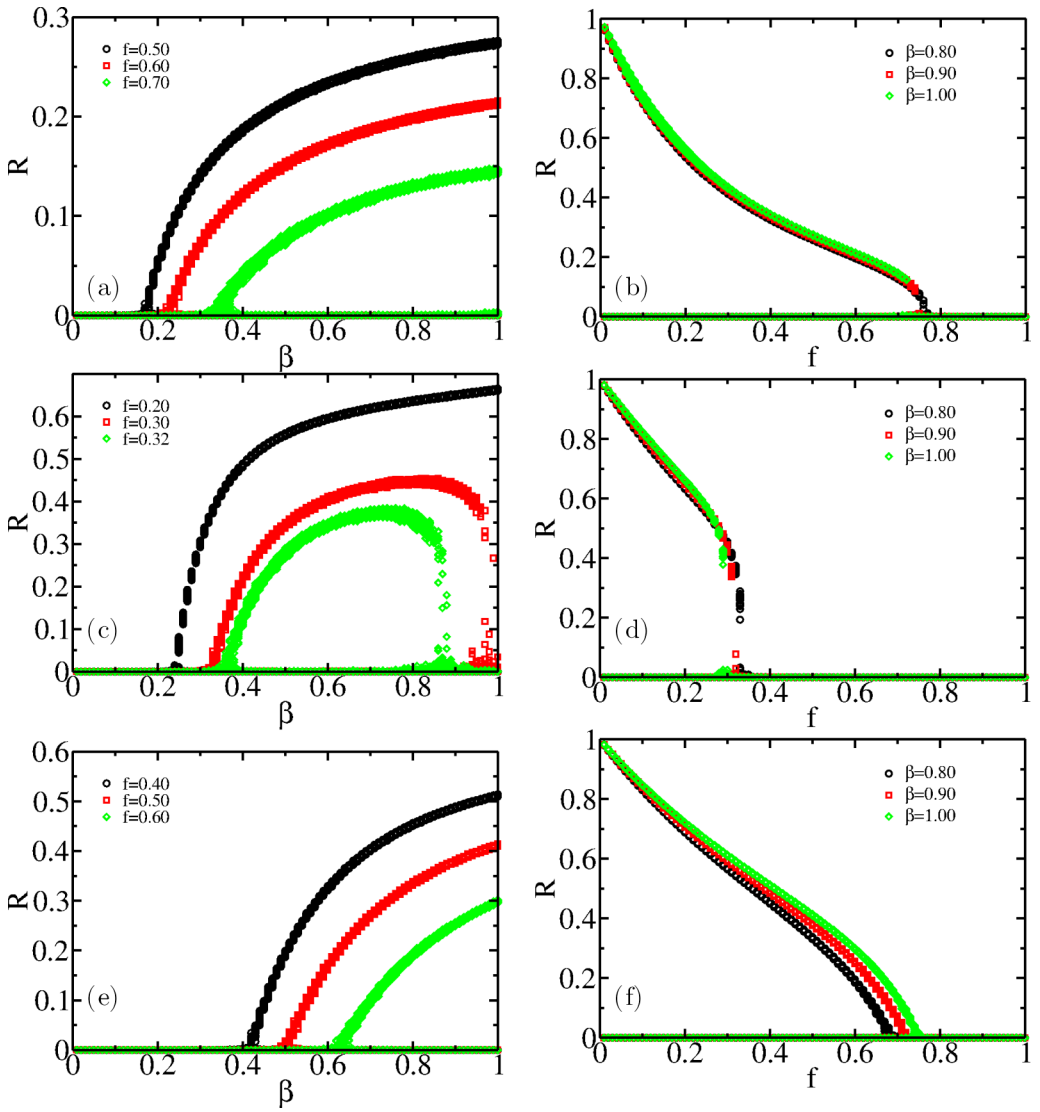

FIG. 8. Scatter plot of the fraction of recovered population R at the final stage as a function of β [(a), (c), (e)], and as a function of f [(b), (d), (f)]. Results were obtained from 10^3 stochastic realizations on RR networks with $k_C = 3$ and $k_I = 7$ [(a) and (b)], $k_C = 5$, $k_I = 2$ [(c) and (d)], and $k_C = 2$, $k_I = 5$ [(e) and (f)].

In contrast to what was observed in Sec. III A, here we do not find any abrupt transition for case III, as shown in Figs. 8(e) and 8(f). This result may be due to the fact that cliques are smaller in case III than in cases I and II, so these cliques have a lower probability of being quarantined. On the other hand, for cases I and II, we obtain that R exhibits an abrupt transition for high values of β, as seen in Figs. 8(b) and 8(d).

In Figs. 9(a)–9(c), we plot the heat-map of the fraction of recovered individuals when an epidemic occurs ($R > 1\%$) in the plane β-f. In these figures, we also include the curve where $R_0 = 1$ [obtained from Eq. (1)]. For all cases, we observe that this curve predicts well the boundary between the epidemic and nonepidemic phases.

Now for case II, we measure

(1) the average size of small outbreaks $\langle s \rangle$ vs β for $f = 0.32$ and different network sizes N_I [see Fig. 10(a)],

(2) the distribution of small outbreak sizes for $\beta = 0.87$ and $f = 0.32$ [see Fig. 10(b)].

As in Figs. 2(b) and 2(c), we can see that $\langle s \rangle$ has a peak around $\beta = 0.87$, and $P(s)$ decays as a power law. Therefore, our findings reveal that outbreaks exhibit features of a continuous phase transition around $\beta = 0.87$ for case II.

2. Nonregular random networks with cliques

So far, we have focused our attention on random networks with cliques in which k_C and k_I follow a delta distribution. In this section, we show results for random networks with cliques in which k_C and k_I follow other probability distributions. Specifically, we consider

(i) a truncated Poisson distribution, defined as

$$\mathrm{Pois}(\lambda, k_{\min}, k_{\max}) = \begin{cases} c\frac{\lambda^k e^{-\lambda}}{k!} & \text{if } k_{\min} \leqslant k \leqslant k_{\max}, \\ 0 & \text{otherwise,} \end{cases} \quad \text{(B1)}$$

where c is a normalization constant;

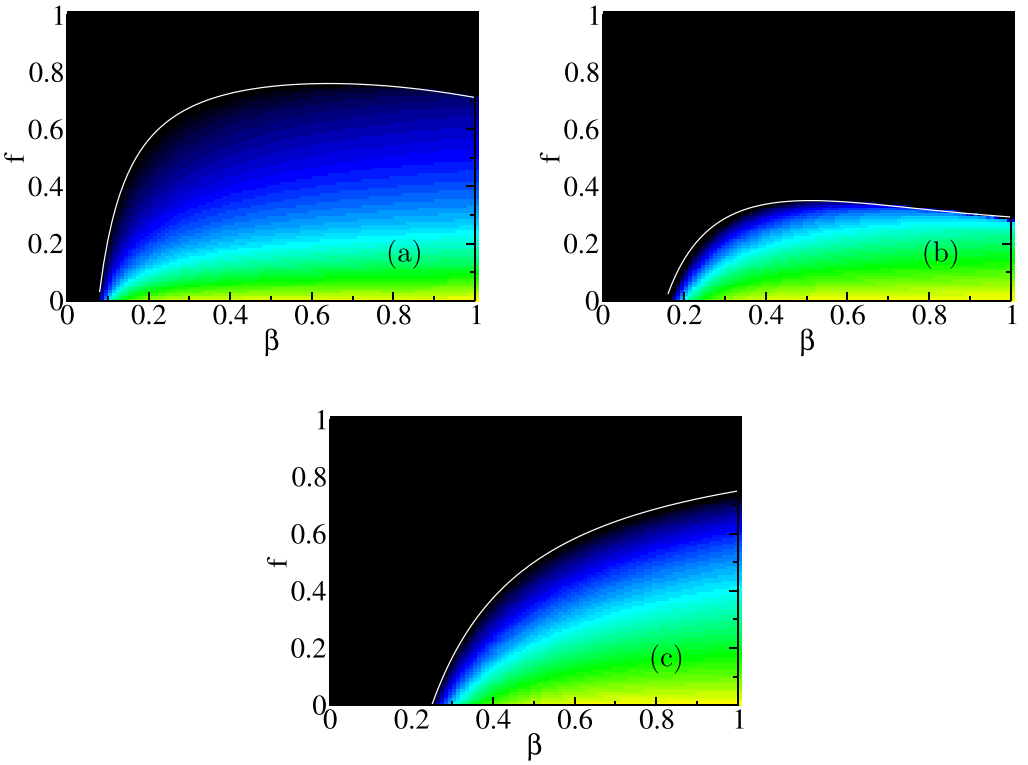

FIG. 9. Heat-map of R in the plane β-f for a RR with cliques with $k_C = 3$ and $k_I = 7$ (a), $k_C = 5$ and $k_I = 2$ (b), and $k_C = 2$ and $k_I = 5$ (c), obtained from stochastic simulations for networks with $N_I = 10^6$. Simulation results were averaged over 10^3 stochastic realizations. The solid white line was obtained from Eq. (1) for $R_0 = 1$.

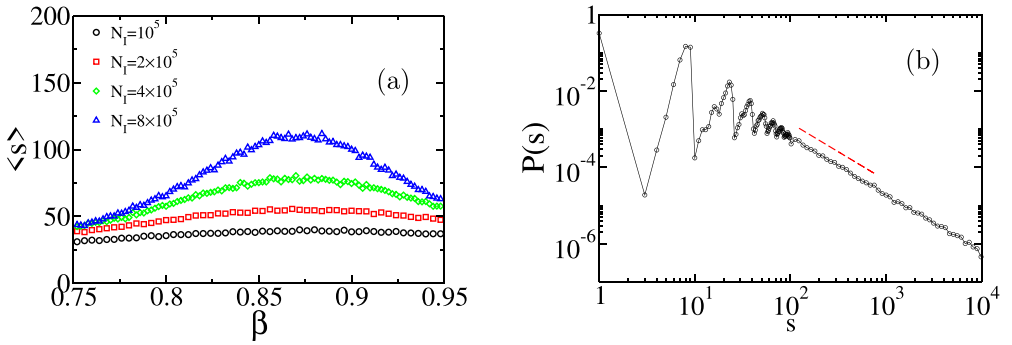

FIG. 10. (a) $\langle s \rangle$ against β (fixing $f = 0.32$) for RR networks with cliques with $k_C = 5$, $k_I = 2$, and several values of N_I. Results were averaged over 10^5 realizations. (b) distribution $P(s)$ for $\beta = 0.87$, $f = 0.32$, and $N_I = 10^6$, obtained from 1.5×10^5 stochastic realizations (symbols). The solid black line is a guide to the eye, and the dashed red line is a power-law function with exponent $\tau - 1 = 1.5$.

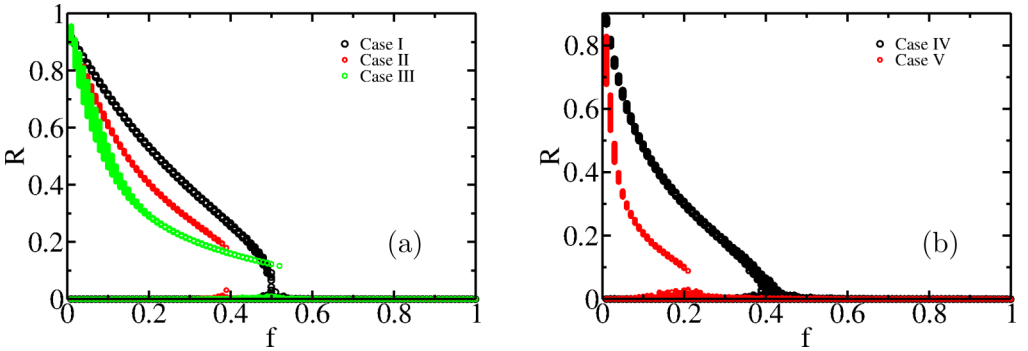

FIG. 11. Scatter plot of the fraction of recovered population R at the final stage as a function of f for cases I–III (a) and cases IV and V (b); see Table I. Results were obtained from 10^3 stochastic realizations on random networks with $N_I = 10^6$.

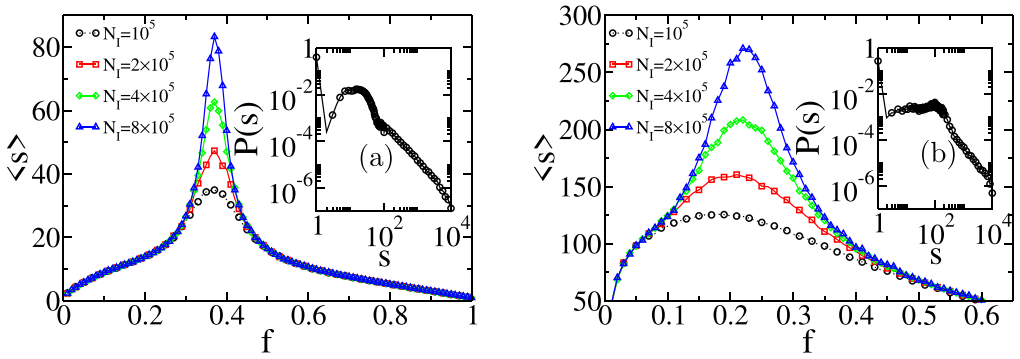

FIG. 12. $\langle s\rangle$ against f (fixing $\beta = 1$) for several values of N_I. Panels (a) and (b) correspond to cases II and V, respectively. Results were averaged over 10^4 realizations. In the insets, we show the distribution $P(s)$ (in log-log scale) for $\beta = 1$, $f = 0.36$, and $N_I = 10^6$ (a) and for $\beta = 1$, $f = 0.22$, and $N_I = 10^6$ (b). These results were averaged over 2×10^5 and 4×10^4 stochastic realizations for panels (a) and (b), respectively. Solid lines are a guide to the eye.

(ii) a truncated power-law distribution, defined as

$$\mathrm{PL}(\lambda, k_{\min}, k_{\max}) = \begin{cases} ck^{-\lambda} & \text{if } k_{\min} \leqslant k \leqslant k_{\max}, \\ 0 & \text{otherwise,} \end{cases} \tag{B2}$$

where c is a normalization constant.

In Figs. 11(a) and 11(b), we plot the fraction of recovered people at the final stage vs f (fixing $\beta = 1$) for the cases listed in Table I. In this table, we also include the mean value of k_C [i.e., $\langle k_C\rangle = \sum_{k_C} k_C P(k_C)$] and its variance [$\mathrm{VAR}(k_C) = \langle k_C^2\rangle - \langle k_C\rangle^2$]:

Similarly to the results in Sec. B 1, from Figs. 11(a) and 11(b) we note that, as the average clique size increases, the system tends to exhibit an abrupt transition.

Now, focusing on cases II and V, in Fig. 12 we plot $\langle s\rangle$ vs f (fixing $\beta = 1$). Additionally, in the insets we show the probability distribution of the final number of recovered people for

(i) $\beta = 1$ and $f = 0.36$ (for case II),

(ii) $\beta = 1$ and $f = 0.22$ (for case V).

As in Sec. III A and Appendix B 1, we obtain that $\langle s\rangle$ has a peak around $f_c(N_I)$ and $P(s)$ decays as a power law, so these results indicate that outbreaks exhibit some features of a continuous phase transition.

In summary, our findings suggest that nonregular networks with larger cliques tend to exhibit features of both discontinuous and continuous phase transitions.

APPENDIX C: PROBABILITY OF A SMALL OUTBREAK

In Sec. III B, we calculated the probability of a small outbreak, $1 - \Pi$, as a function of f (with $\beta = 1$) for the case in which k_C and k_I follow a delta distribution. Here, we will generalize our previous equations to compute $1 - \Pi$ for any arbitrary probability distributions $P(k_C)$ and $P(k_I)$.

Let us consider a random network with cliques that can be represented by a bipartite network. We define the following generating functions:

(1) $G_{0C}[x] = \sum_{k_C} P(k_C)x^{k_C}$, which is the generating function for the distribution $P(k_C)$, and $G_{1C}[x] = \sum_{k_C} k_C P(k_C)/\langle k_C\rangle x^{k_C-1}$ which is the generating function for the distribution $k_C P(k_C)/\langle k_C\rangle$,

(2) $G_{0I}[x] = \sum_{k_I} P(k_I)x^{k_I}$, which is the generating function for the distribution $P(k_I)$, and $G_{1I}[x] = \sum_{k_I} k_I P(k_I)/\langle k_I\rangle x^{k_I-1}$ which is the generating function for the distribution $k_I P(k_I)/\langle k_I\rangle$.

In the same way as in Sec. III B, we define ϕ as the probability that an infected individual (reached by a link) does not generate an epidemic. For any arbitrary distribution $P(k_C)$ and $P(k_I)$, we have that ϕ obeys the following equation:

$$\phi = G_{1I}[G_{1C}[(1-f)\phi] + 1 - G_{1C}[1-f]], \tag{C1}$$

$$= \sum_{k_I} \frac{k_I P(k_I)}{\langle k_I\rangle} \{G_{1C}[(1-f)\phi] + 1 - G_{1C}[1-f]\}^{k_I-1}, \tag{C2}$$

The right-hand side of the above equation is the probability that an individual "j" (reached through a link) does not generate an epidemic. This is due to the fact that none of the $k_I - 1$ outgoing cliques generates an epidemic, because one of the following two events occurs in every clique:

(1) The outgoing clique has at least one infected member who is detected with probability $1 - G_{1C}[1-f]$, so the entire clique is quarantined.

(2) The outgoing clique is not isolated, but it will not be able to cause an epidemic with probability $G_{1C}[(1-f)\phi]$.

On the other hand, the probability $1 - \Pi$ that a randomly chosen individual will not generate an epidemic is given by

$$1 - \Pi = f + (1-f)G_{0I}[G_{1C}[(1-f)\phi] + 1 - G_{1C}[1-f]], \tag{C3}$$

where the second term on the right-hand side of this equation has an interpretation similar to that of Eq. (C1). Following a procedure similar to that in Sec. III B, it can be seen that the critical probability of detection f_c at which a phase transition occurs is implicitly given by

$$1 = (1-f_c)G'_{1I}(1)G'_{1C}[(1-f_c)], \tag{C4}$$

where $G'_{1I}(x) \equiv dG_{1I}/dx$ and $G'_{1C}(x) \equiv dG_{1C}/dx$. In particular, for the case where k_C and k_I follow a Poisson distribution [i.e., $\mathrm{Pois}(\lambda, 0, \infty)$], the above equation can be solved

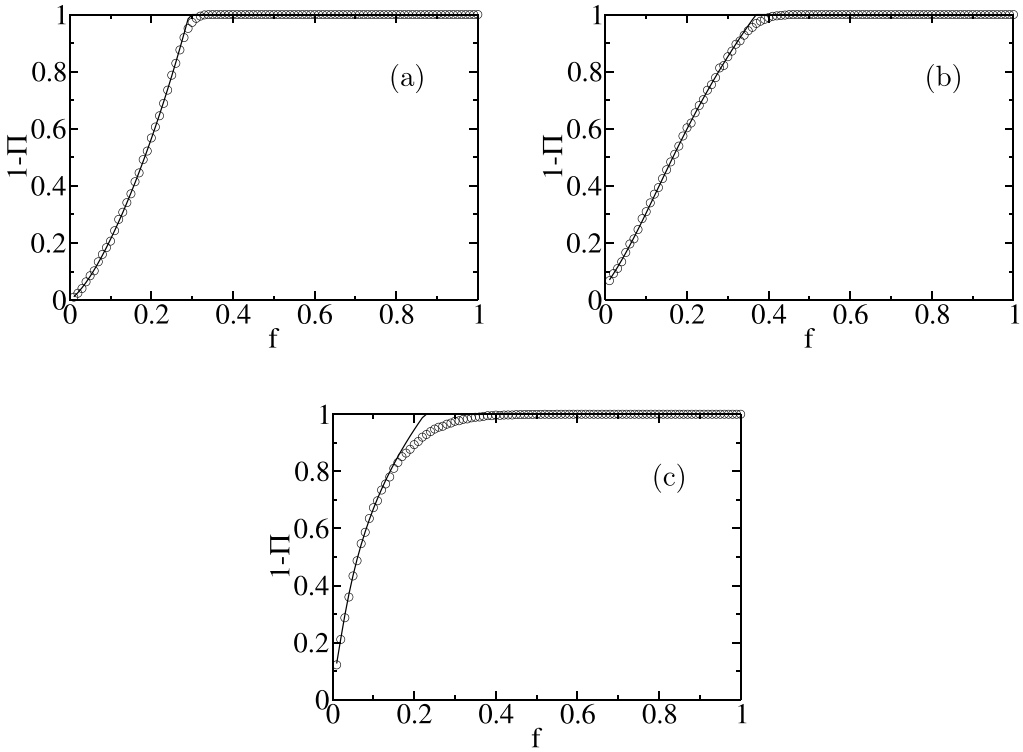

FIG. 13. Probability of a small outbreak $(1-\Pi)$ vs f for $\beta = 1$ and several network topologies: RR networks with $P(k_C) = \delta_{k_C,5}$ and $P(k_I) = \delta_{k_I,2}$ (a), non-RR networks with $P(k_C) = \text{Pois}(7, 0, 20)$ and $P(k_I) = \text{Pois}(3, 0, 20)$ (b), and non-RR networks with $P(k_C) = \text{PL}(1.5, 2, 100)$ and $P(k_I) = \text{Pois}(3, 0, 20)$ (c). The line corresponds to the theory given by Eqs. (C1)–(C3), and symbols are simulation results averaged over 10^4 network realizations with $N_I = 10^5$.

explicitly in terms of the Lambert W function [56]:

$$f_c = 1 - \frac{W\left(\frac{e^{\langle k_C\rangle}}{\langle k_I\rangle}\right)}{\langle k_C\rangle}. \tag{C5}$$

To see the validity of our equations, we run numerical simulations for the following networks:

case I: RR networks with $P(k_C) = \delta_{k_C,5}$ and $P(k_I) = \delta_{k_I,2}$, where $f_c = 0.293$ [computed from Eq. (C4)],

case II: non-RR networks with $P(k_C) = \text{Pois}(7, 0, 20)$ and $P(k_I) = \text{Pois}(3, 0, 20)$, where $f_c = 0.369$,

case III: non-RR networks with $P(k_C) = \text{PL}(1.5, 2, 100)$ and $P(k_I) = \text{Pois}(3, 0, 20)$, where $f_c = 0.226$.

In Fig. 13, we show the probability of an outbreak as a function of f (with $\beta = 1$) obtained from our simulations and Eqs. (C1)-(C3). As we can see, the agreement between theory and simulations is excellent.

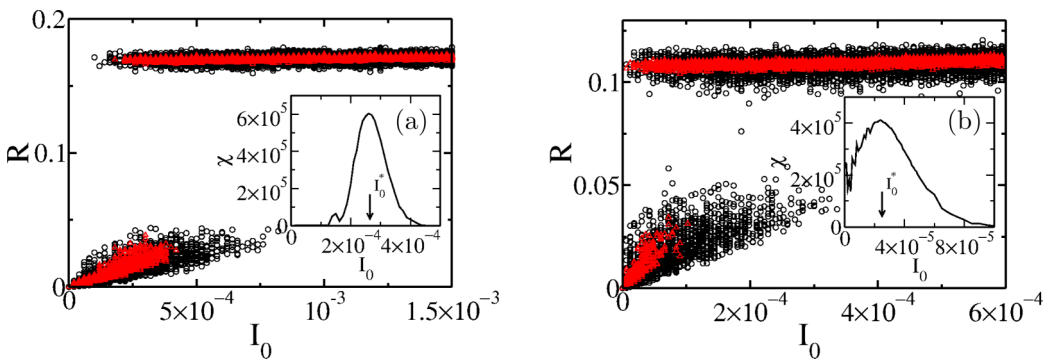

FIG. 14. Scatter plot of R vs I_0 (fixing $\beta = 1$) obtained from numerical simulations on random networks where $P(k_C) = \text{Pois}(7, 0, 20)$ and $P(k_I) = \text{Pois}(3, 0, 20)$ (a) and $P(k_C) = \text{PL}(1.5, 2, 100)$ and $P(k_I) = \text{Pois}(3, 0, 20)$ (b). We set the probability of detection to $f = 0.40$ for panel (a), and $f = 0.25$ for panel (b). Note that in both cases we used $f > f_c$ (see the value of f_c in Appendix C). Numerical results were obtained from 10^3 stochastic realizations (a) and 3×10^3 stochastic realizations (b) on networks with $N_I = 10^6$ (black symbols) and $N_I = 8 \times 10^6$ (red symbols). The insets show the susceptibility of the number of recovered people, χ, as a function of I_0 (for $N_I = 8 \times 10^6$), where I_0^* is the peak position.

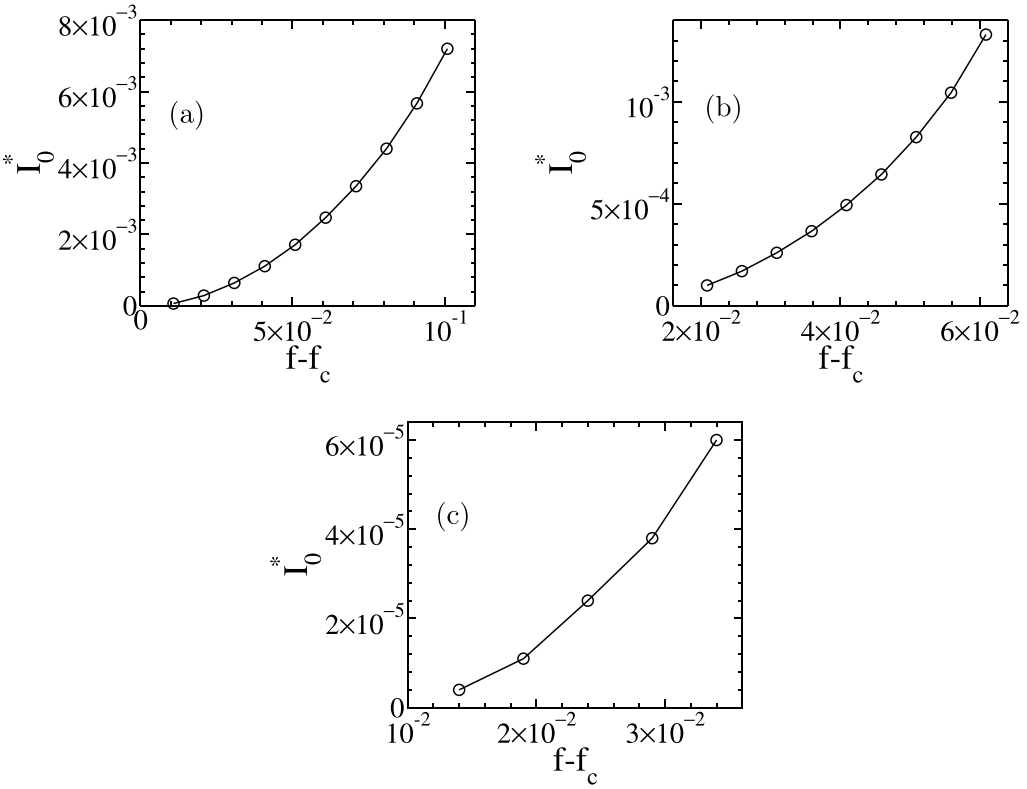

FIG. 15. I_0^* as a function of $f - f_c$ (fixing $\beta = 1$) for random networks with cliques where $P(k_C) = \delta_{k_C,7}$ and $P(k_I) = \delta_{k_I,3}$ (a), $P(k_C) =$ Pois(7, 0, 20) and $P(k_I) =$ Pois(3, 0, 20) (b), and $P(k_C) =$ PL(1.5, 2, 100) and $P(k_I) =$ Pois(3, 0, 20) (c). Symbols represent simulation results in networks with $N_I = 8 \times 10^6$ and solid lines are a guide to the eye. The number of realizations was 250 (a), 1000 (b), and 3000 (c).

APPENDIX D: BACKWARD BIFURCATION: ADDITIONAL RESULTS

In Sec. III C, we found (for $\beta = 1$) that a backward bifurcation phenomenon emerges for RR networks with cliques with $k_C = 7$ and $k_I = 3$. Here, we will show that this phenomenon also occurs on networks where k_C and k_I follow other probability distributions.

In Fig. 14, we plot the fraction of recovered individuals at the final stage as a function of I_0 (fixing $\beta = 1$) for the following cases:

case I: $P(k_C) =$ Pois(7, 0, 20) and $P(k_I) =$ Pois(3, 0, 20),

case II: $P(k_C) =$ PL(1.5, 2, 100) and $P(k_I) =$ Pois(3, 0, 20).

As in Sec. III C, we can see that R exhibits an abrupt jump around a threshold I_0^* for $\beta = 1$, where I_0^* is the peak position of the susceptibility [55], defined as

$$\chi = N_I \frac{\langle R^2 \rangle - \langle R \rangle^2}{\langle R \rangle}. \tag{D1}$$

Similar results can be obtained for $\beta = 0.8$ and $\beta = 0.9$ (not shown here).

Finally, in Fig. 15, we display the threshold I_0^* vs $f - f_c$ for different network structures.

[1] S. Flaxman, S. Mishra, A. Gandy, H. J. T. Unwin, T. A. Mellan, H. Coupland, C. Whittaker, H. Zhu, T. Berah, J. W. Eaton *et al.*, Nature (London) **584**, 257 (2020).

[2] M. W. Fong, H. Gao, J. Y. Wong, J. Xiao, E. Y. Shiu, S. Ryu, and B. J. Cowling, Emerg. Infect. Dis. **26**, 976 (2020).

[3] H. Markel, H. B. Lipman, J. A. Navarro, A. Sloan, J. R. Michalsen, A. M. Stern, and M. S. Cetron, JAMA **298**, 644 (2007).

[4] P. De, A. E. Singh, T. Wong, W. Yacoub, and A. Jolly, Sex. Transm. Infect. **80**, 280 (2004).

[5] Z. Susswein and S. Bansal, medRxiv, doi: 10.1101/2020.12.08.20246082.

[6] D. A. Luke and J. K. Harris, Annu. Rev. Public Health **28**, 69 (2007).

[7] Z. Wang, M. A. Andrews, Z.-X. Wu, L. Wang, and C. T. Bauch, Phys. Life Rev. **15**, 1 (2015).

[8] X. Wang, Q. An, Z. He, and W. Fang, Complexity **2021**, 3816221 (2021).

[9] S. Kojaku, L. Hébert-Dufresne, E. Mones, S. Lehmann, and Y.-Y. Ahn, Nat. Phys. **17**, 652 (2021).

[10] A. K. Rizi, A. Faqeeh, A. Badie-Modiri, and M. Kivelä, Phys. Rev. E **105**, 044313 (2022).

[11] G. St-Onge, V. Thibeault, A. Allard, L. J. Dubé, and L. Hébert-Dufresne, Phys. Rev. Lett. **126**, 098301 (2021).

[12] G. St-Onge, V. Thibeault, A. Allard, L. J. Dubé, and L. Hébert-Dufresne, Phys. Rev. E **103**, 032301 (2021).

[13] T. Gross, C. J. D. D'Lima, and B. Blasius, Phys. Rev. Lett. **96**, 208701 (2006).

[14] R. Durrett and D. Yao, Electron. J. Probab. **27**, 1 (2022).
[15] F. Ball and T. Britton, Random Struct. Algorithms **61**, 250 (2022).
[16] G. Strona and C. Castellano, Phys. Rev. E **97**, 022308 (2018).
[17] C. Vyasarayani and A. Chatterjee, Nonlinear Dyn. **101**, 1653 (2020).
[18] T. Hasegawa and K. Nemoto, Phys. Rev. E **96**, 022311 (2017).
[19] G. Börner, M. Schröder, D. Scarselli, N. B. Budanur, B. Hof, and M. Timme, J. Phys. Complex. **3**, 04LT02 (2022).
[20] M. Molloy and B. Reed, Comb. Probab. Comput. **7**, 295 (1998).
[21] M. Molloy and B. Reed, Random Struct. Algorithms **6**, 161 (1995).
[22] B. Karrer and M. E. J. Newman, Phys. Rev. E **82**, 066118 (2010).
[23] M. E. J. Newman, Phys. Rev. E **66**, 016128 (2002).
[24] F. Radicchi and G. Bianconi, Phys. Rev. E **102**, 052309 (2020).
[25] J. C. Miller, PLoS ONE **9**, e101421 (2014).
[26] P. Krapivsky, J. Stat. Mech. (2021) 013501.
[27] G. Machado and G. J. Baxter, Phys. Rev. E **106**, 014307 (2022).
[28] T. Hasegawa and K. Nemoto, Phys. Rev. E **93**, 032324 (2016).
[29] *Mathematical Epidemiology*, edited by F. Brauer, P. Van den Driessche, J. Wu, and L. J. Allen, Lecture Notes in Mathematics Vol. 1945 (Springer, Berlin, 2008).
[30] D. Stauffer and A. Aharony, *Introduction to Percolation Theory*, revised 2nd ed. (CRC Press, Boca Raton, FL, 2014).
[31] P. Grassberger, Math. Biosci. **63**, 157 (1983).
[32] It is worth noting that the process under study is non-Markovian, and infected individuals recover with probability 1 after t_r time steps.
[33] F. Battiston, G. Cencetti, I. Iacopini, V. Latora, M. Lucas, A. Patania, J.-G. Young, and G. Petri, Phys. Rep. **874**, 1 (2020).
[34] F. Battiston, E. Amico, A. Barrat, G. Bianconi, G. Ferraz de Arruda, B. Franceschiello, I. Iacopini, S. Kéfi, V. Latora, Y. Moreno *et al.*, Nat. Phys. **17**, 1093 (2021).
[35] E. Kenah and J. M. Robins, Phys. Rev. E **76**, 036113 (2007).
[36] L. A. Meyers, M. Newman, and B. Pourbohloul, J. Theor. Biol. **240**, 400 (2006).
[37] J. C. Miller, J. R. Soc. Interface **6**, 1121 (2009).
[38] L. D. Valdez, L. A. Braunstein, and S. Havlin, Phys. Rev. E **101**, 032309 (2020).
[39] S. V. Buldyrev, R. Parshani, G. Paul, H. E. Stanley, and S. Havlin, Nature (London) **464**, 1025 (2010).
[40] L. D. Valdez, L. Shekhtman, C. E. La Rocca, X. Zhang, S. V. Buldyrev, P. A. Trunfio, L. A. Braunstein, and S. Havlin, J. Complex Netw. **8**, cnaa013 (2020).
[41] R. Pastor-Satorras, C. Castellano, P. Van Mieghem, and A. Vespignani, Rev. Mod. Phys. **87**, 925 (2015).
[42] W. Wang, Z.-X. Wang, and S.-M. Cai, Phys. Rev. E **98**, 052312 (2018).
[43] G. Dong, F. Wang, L. M. Shekhtman, M. M. Danziger, J. Fan, R. Du, J. Liu, L. Tian, H. E. Stanley, and S. Havlin, Proc. Natl. Acad. Sci. USA **118**, e1922831118 (2021).
[44] R. Cohen, S. Havlin, and D. ben Avraham, in *Handbook of Graphs and Networks: From the Genome to the Internet* (Wiley, New York, 2002), pp. 85–110.
[45] G. J. Baxter, S. N. Dorogovtsev, A. V. Goltsev, and J. F. F. Mendes, Phys. Rev. E **83**, 051134 (2011).
[46] M. A. Di Muro, L. D. Valdez, H. E. Stanley, S. V. Buldyrev, and L. A. Braunstein, Phys. Rev. E **99**, 022311 (2019).
[47] Y. Shang, Phys. Rev. E **89**, 012813 (2014).
[48] L. D. Valdez and L. Braunstein, Physica A **594**, 127057 (2022).
[49] P. Mann, V. A. Smith, J. B. O. Mitchell, and S. Dobson, Phys. Rev. E **103**, 012309 (2021).
[50] P. Mann, V. A. Smith, J. B. O. Mitchell, C. Jefferson, and S. Dobson, Phys. Rev. E **104**, 024304 (2021).
[51] A. Allard, L. Hébert-Dufresne, P.-A. Noël, V. Marceau, and L. J. Dubé, J. Phys. A: Math. Theor. **45**, 405005 (2012).
[52] J. P. Gleeson, Phys. Rev. E **80**, 036107 (2009).
[53] A. B. Gumel, J. Math. Anal. Appl. **395**, 355 (2012).
[54] D. Ludwig, Math. Biosci. **23**, 33 (1975).
[55] S. C. Ferreira, C. Castellano, and R. Pastor-Satorras, Phys. Rev. E **86**, 041125 (2012).
[56] Here, we use the principal branch of the Lambert function.